FULL PAPER

Perovskite Photovoltaics for Dim-Light Applications

*Chien-Yu Chen, Jung-Hao Chang, Kai-Ming Chiang, Hong-Lin Lin, Sheng-Yi Hsiao, and Hao-Wu Lin**

The use of photovoltaic cells with an organometallic perovskite as the active layer for indoor dim-light energy harvesting is evaluated. By designing the electron-transporting materials and fabrication processes, the traps in the perovskite active layers and carrier dynamics can be controlled, and efficient devices are demonstrated. The best-performing small-area perovskite photovoltaics exhibit a promising high power conversion efficiency up to ≈27.4%, no hysteresis behavior, and an exceptionally low maximum power point voltage variation of ≈0.1 V under fluorescent lamp illumination at 100–1000 lux. The 5.44 cm^2 large-area device also shows a high efficiency of 20.4% and a promising long-term stability. Compared with the most efficient inorganic and organic solar cells nowadays, the competitive efficiency, low fabrication cost, and low raw material costs make perovskite photovoltaics ideal for indoor light harvesting and as Internet of Things power provider.

1. Introduction

Recently, dim light, especially indoor energy harvesting, has attracted great attention because of the unprecedented development of the Internet of Things (IoT).[1–3] IoT promises a future where a wide variety of physical objects, such as consumer electronics, sensing nodes, household furniture, and personal belongings will be connected to the internet and be able to sense and interact with their internal states or the external environment. As these objects are integrated with wireless communication systems and sensors, and they are usually separated from the electrical grid, off-grid power systems are essential. Among all the harvesting technologies of various types of energy sources, including piezoelectricity, vibrational energy, and thermoelectricity, photovoltaics (PVs) show great potential and can deliver a much larger (by several orders of magnitude) energy density than any other technique.[4] Thus, the recent evolution of PVs not only targets 1 sun (100 mW cm^{-2}) to several sun solar applications but also dim-light conditions, for which the light intensity is 100–1000 times lower than 1 sun and the illumination spectrum is limited to the visible wavelength range provided by fluorescent lamps or light-emitting diodes (LEDs). Excitonic PVs, such as organic solar cells (OSCs) and dye-sensitized solar cells (DSSCs) that can maintain high photovoltage and cell efficiency under dim-light illumination, have long been regarded as the most promising candidates for this application.[5,6]

Along with these new light-harvesting devices, organometallic perovskite PVs (PePVs) have recently attracted even more attentions because of their special material properties, outstanding performance, low-temperature large-area production capability, and short energy payback time.[7–15] Furthermore, the bandgap of organometallic perovskite materials can be freely tuned between 1.2 and 3.1 eV by incorporating varied halides, organic ions, and metals for particular applications. Theoretical calculations have suggested an optimal bandgap of 1.9 eV for modern indoor lighting sources,[16] making organometallic perovskites particularly interesting to achieve an optimum efficiency by bandgap engineering. Despite all the favorable characteristics of PePVs for indoor dim-light applications, the cell performance of PePVs under indoor dim-light conditions and device engineering dedicated to this application have not been reported. In this report, we experimentally demonstrate that PePVs exhibit excellent dim-light performance. By judiciously controlling the materials and fabrication of the electron-transporting layers (ETLs) of the devices, which effectively eliminate the traps in the perovskite active layer, the optimized devices exhibited sustained characteristics (high open-circuit voltage (V_{OC}) and high fill factor (FF) even at a very low light intensity of 100 lux). Small-area lab cells with the optimized structure delivered power conversion efficiencies (PCEs) of 22.5%–27.4% under illumination intensities of 100–1000 lux from a T5 fluorescent light of 6500 K color temperature. A large-area device with a device area of 5.44 cm^2 exhibited an impressive PCE up to ≈20.4% under an illumination intensity of 600–1000 lux, which is comparable to that of the highest reported expensive GaAs and AlGaAs cells (19.4% and 21.1%, respectively) and commercially available state-of-the-art DSSC, OSC submodules (14.1% and 14.3%).

Compared with solar irradiation, indoor light sources exhibit distinct spectra and intensities. The majority of indoor light sources today are fluorescent lamps, with the market share of solid-state LEDs gradually increasing. **Figure 1** presents the illumination spectra of a 6500 K T5 fluorescent lamp and a white LED lamp along with the standard AM 1.5G solar spectrum and a typical external quantum efficiency (EQE) spectrum of PePVs.[17] Both fluorescent and LED lamps exhibit illumination wavelength ranges from 350 to 750 nm. With a bandgap of

C.-Y. Chen, J.-H. Chang, K.-M. Chiang, H.-L. Lin, S.-Y. Hsiao, Prof. H.-W. Lin
Department of Materials Science and Engineering
National Tsing Hua University
Hsinchu 30013, Taiwan
E-mail: hwlin@mx.nthu.edu.tw

DOI: 10.1002/adfm.201503448

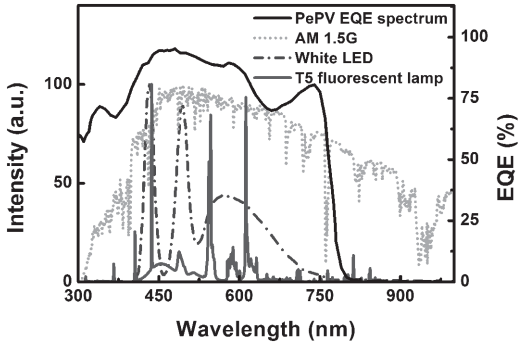

Figure 1. Illumination spectra of AM 1.5G, a fluorescent lamp, and a white LED and a typical PePV EQE spectrum.

≈1.6 eV, the spectral response of the $CH_3NH_3PbI_{3-x}Cl_x$ PePVs in this study nicely covers the entire spectra. However, when the PePVs are used as solar cells, considerable photon loss in the infrared range is anticipated. This phenomenon indicates that PePVs could be better suited as indoor energy sources than as solar cells. However, only if the PePVs also maintain a high V_{OC} and FF under dim-light illumination can the devices exhibit good performance for indoor applications, which largely depends on the PV mechanism of perovskite materials, effective carrier trap control, and device engineering. Office and household lighting ranges from ≈100 to ≈1000 lux. With a 6500 K fluorescent lamp spectrum, these illuminances correspond to 31–310 μW cm^{-2} light intensity, which is three orders of magnitude lower than 1 sun radiation (100 mW cm^{-2}).

In this article, we explore the performance of PePVs under fluorescent lamp illumination. Moreover, in recent studies in the literature, trap control in the perovskite layer was observed to be important for perovskite solar cells operated in bright light.[18–20] With the greatly reduced amount of photon carriers generated in dim light, we believe that traps in the active layer may play an even more critical role in dim light than in solar cells. Hence, ETL fabrication was carefully performed with the aim of reducing the trap density in the perovskite layers.

2. Results and Discussion

2.1. Device Design and Characterization

Inverted cells with a typical structure of indium tin oxide (ITO) (140 nm)/poly(3,4-ethylenedioxythiophene) polystyrene sulfonate (PEDOT:PSS) (40 nm)/perovskite (≈250 nm)/ETL (≈120 nm)/1,3,5-tri(*m*-pyrid-3-yl-phenyl)benzene (TmPyPB) (7 nm)/Ag (150 nm) were used in this study. PEDOT:PSS was used as a hole-transporting layer, and TmPyPB was utilized as an electron-transporting cathode buffer.[21] Fullerene-based ETLs are usually used in inverted perovskite solar cells because of the efficient charge transfer between the fullerene layer and perovskite layer.[22] Both solution-processed [6,6]-phenyl-C_{61}-butyric acid methyl ester (PCBM) and vacuum-deposited fullerenes have been utilized, and they exhibited matched efficiency under 1 sun illumination.[23,24] However, as observed in **Figure 2**a–c, the device utilizing the solution-processed PCBM exhibited a considerably higher efficiency and distinguished current density to voltage (*J*–*V*) characteristics compared with the cells using vacuum-deposited C_{60} and C_{70} as the ETL under indoor illumination. It is believed that the traps at the perovskite surface and grain boundaries can be filled by the penetrated solution-processed PCBM upper layer, whereas the vacuum-deposited fullerenes only evenly covered the perovskite films, as illustrated in Figure 2d–f. Figure S1 in the Supporting Information presents scanning electron microscopy (SEM) images of the PePVs with different fullerenes as ETLs.[18,25,26] The device using C_{60} as the ETL exhibited a V_{OC} of 0.72 V and an FF of 0.60 at 1000 lux; however, these values decreased to a V_{OC} of 0.51 V and an FF of 0.35 at 100 lux. The cells utilizing larger C_{70} fullerene exhibited even poorer performance of V_{OC} = 0.59 V and 0.49 FF at 1000 lux, and these values largely decreased to V_{OC} = 0.25 V and 0.27 FF at 100 lux. In contrast, the PePVs with the solution-processed PCBM ETL exhibited a decent PCE of 26.0%, a V_{OC} of 0.77 V, and an FF of 0.77 at 1000 lux and a slight performance decrease to 20.5% PCE, V_{OC} = 0.68 V, and 0.68 FF even at 100 lux. These results clearly indicate that the trap-filling phenomenon, which was verified later by photophysical measurements, can greatly improve the performance of PePVs operated in dim light.

We then further optimized the fabrication process of the PCBM ETL using a two-step deposition. In the first step, a dilute PCBM solution (3 mg mL^{-1}) was spun coated on the perovskite layer before the thermal annealing of the perovskite film. This small amount of PCBM was intended to more effectively fill the traps when the perovskite crystal was formed upon the thermal annealing. Later, during the second step, after thermal annealing of the perovskite layer, a dense PCBM solution (30 mg mL^{-1}) was further spun coated to create a 120 nm ETL for electron transporting and pinhole filling. The device performance and illustration of improved PCBM penetration into the perovskite layer are illustrated in **Figure 3**a,b, respectively. The two-step PCBM cells exhibited better performance than the one-step PCBM device with excellent PCE values up to 27.4% at 1000 lux and 22.5% at 100 lux. The performance of all the devices is summarized in **Table 1** (100, 600, and 1000 lux) and Table S1 in the Supporting Information (all luminance levels).

As demonstrated in Figures 2a–c and 3a, notably, the C_{60} and C_{70} ETL devices exhibited a slight hysteresis behavior, and both the one-step and two-step PCBM ETL devices exhibited no hysteresis with different voltage sweeping directions. These results may indicate that the notorious hysteresis characteristics of perovskite solar cells are more likely to occur at higher illumination intensity and thus at higher carrier density. To date, almost all the PePVs' hysteresis measurements were performed under 1 sun illumination. We believe that incident-light-dependent hysteresis characteristics may provide additional information for better understanding the origin of the various hysteresis observed in perovskite solar cells.[27–29]

Compared with recently published record-high AlGaAs and GaAs dim-light PV devices, which exhibit PCEs and V_{OC} values of 21.1%, 0.84 V and 19.4%, 0.66 V, respectively, the optimized PePVs deliver a competitive efficiency and high photovoltage of 26.4% and 0.84 V at a similar luminance of ≈600 lux.[30,31] With the low-cost large-area solution process and simple thermal evaporation, PePVs can be easily regarded as one of the most promising candidates for indoor energy harvesting.

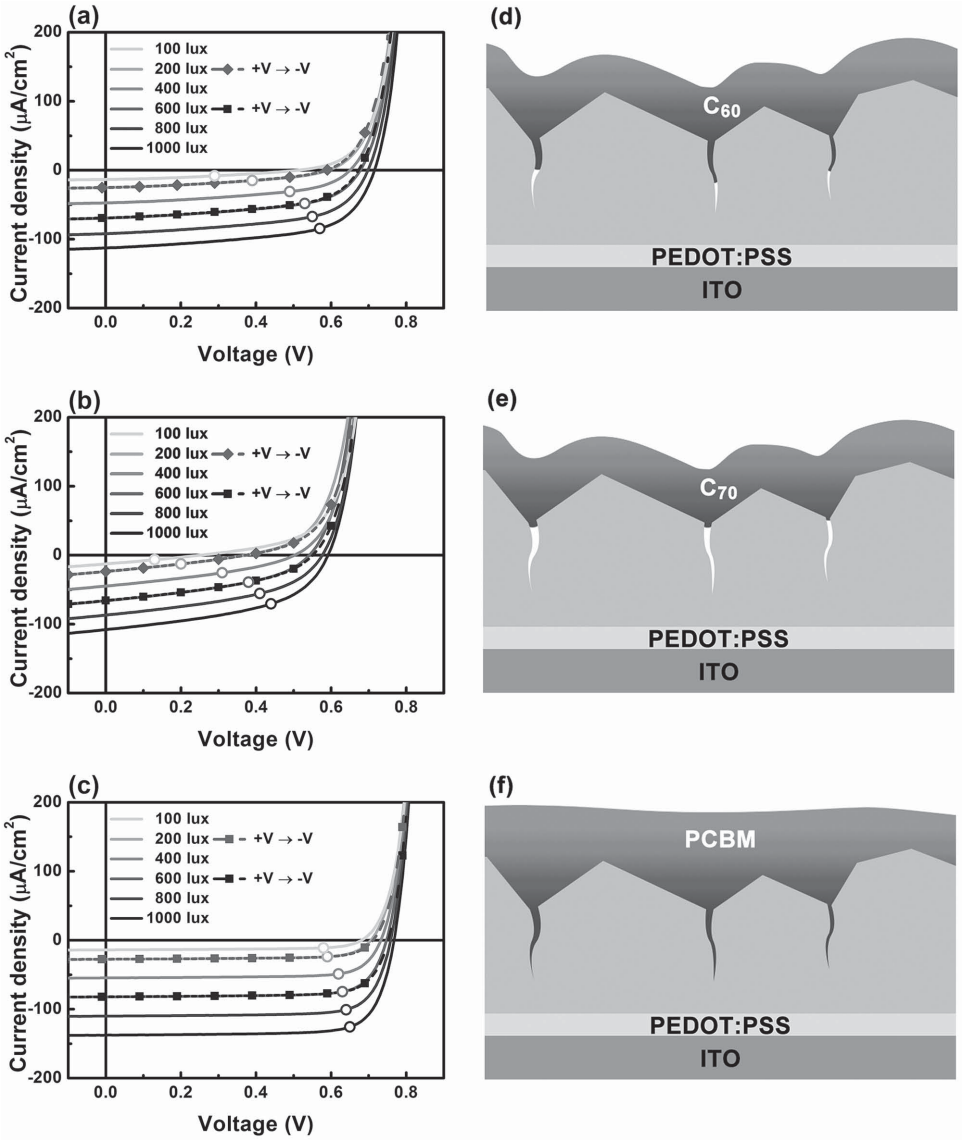

Figure 2. *J–V* characteristics of PePVs with a) C_{60}, b) C_{70}, and c) PCBM as ETLs. The open-circle symbols indicate the MPPs of the device. The solid lines and dashed lines represent the scanning direction from negative to positive bias and from positive to negative bias, respectively. d–f) Schematic illustrations of PePVs with different ETLs.

Because in normal operation, the intensity of indoor illumination may vary more than one order of the magnitude, if the maximum power points (MPPs) deviate largely with the intensity of the illumination, complicated MPP tracking (MPPT) circuits are needed to ensure that the device provides the highest power to external circuitry.[32–34] Nevertheless, if the MPPs or, more specifically, the operational voltages of the MPPs remain constant regardless of the incident light intensity, a much simpler MPPT circuit can be used, and the operational point can be defined by selecting the resistance value of a single resistor.[35,36] Thus, the stability of the voltage at the MPPs under various illumination intensities is another important parameter for indoor PV cells. The MPPs of the devices are represented by open-circle symbols in Figure 2a–c and Figure 3a. The two-step PCBM cells exhibited an exceptionally low MPP voltage variation (ΔV_{MPP}) of ≈0.1 V from 100 to 1000 lux. This finding indicates that a low-cost simple MPPT circuit can be used together with low-cost PePVs to create a cost-competitive energy harvesting total solution.

2.2. Photophysical Properties

To investigate the origin of the large efficiency variation of the devices with different ETLs, we performed transient photocurrent (TPC) and impedance spectroscopy measurements. As demonstrated in **Figure 4**a, the device utilizing PCBM as the ETL exhibited faster transient photocurrent decay than C_{60} and C_{70}, and the two-step PCBM device exhibited the fastest decay rate of down to 0.21 μs. The fast transient photocurrent

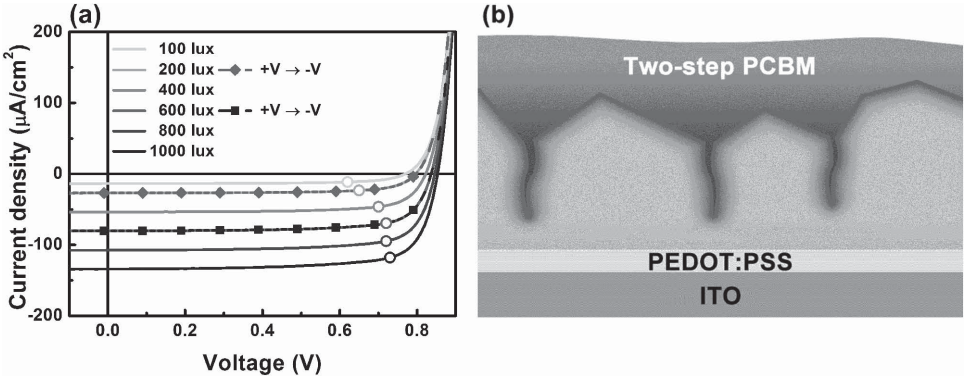

Figure 3. a) *J–V* characteristics of PePV with two-step PCBM as the ETL. The solid lines and dashed lines represent the scanning direction from negative to positive bias and from positive to negative bias, respectively. b) Schematic illustration of PePV with two-step PCBM as the ETL.

decay rate generally indicates efficient carrier sweep-out and carrier collection.[37,38] However, the mobility of vacuum-deposited C_{60} is higher than that of PCBM, and furthermore, the mobility of perovskite thin films is much higher than that of fullerenes.[39–41] Hence, our results indicate that the bottleneck of carrier transport in PePVs is not in the 120 nm thick fullerene ETLs but possibly in hard-to-mobilize trapped carriers at the perovskite/ETL interfaces.[42,43] Proper trap-filling engineering (e.g., optimization of ETL materials and fabrication) to eliminate these traps can largely increase the carrier sweep-out rate.

Impedance spectroscopy was conducted near V_{OC} over the range of 100 kHz to 0.1 Hz under 600 lux illumination, and the results are presented in Figure 4b. The inset of Figure 4b shows the equivalent circuit used for the fitting.[44] The internal series resistance (R_s) is attributed to the ITO anode and counter electrode, and R_{CT} refers to the charge-transfer resistance within the bulk perovskite layer and at the perovskite/carrier transporting layer interface.[45] R_{CT} of the one-step PCBM perovskite device was 11.3 kΩ, which was lower than the values of 15.4 kΩ and 15.8 kΩ of the C_{60} and C_{70} ETL devices, respectively, and was further reduced to 7.27 kΩ in the two-step PCBM device. The low R_{CT} value implies smooth carrier transport at the interface between the perovskite and ETL. Together with the TPC results, we believe that using a two-step PCBM ETL process, PCBM can successfully penetrate into the perovskite layer and fill the defects of perovskite grain boundaries, which eliminate traps in perovskite layers. The effect is believed to be more important in dim-light situations. In bright 1 sun illumination, the traps in the perovskite layers may eventually be filled by the large amount of photocarriers. This phenomenon explains the similar performance of PePVs under bright-light illumination regardless of the ETL materials. However, in dim-light conditions, and thus in low-photocarrier-density conditions, traps in the perovskite layer could dominate the performance of PePVs.

Table 1. PV parameters utilizing different ETLs under indoor illumination.

	ETL	V_{OC} [V]	J_{SC} [μA cm^{-2}]	FF	PCE (highest) [%]
100 lux					
	Two-step PCBM	0.75 ± 0.03	13.57 ± 1.66	0.65 ± 0.03	20.9 ± 1.4 (22.5)
	One-step PCBM	0.67 ± 0.02	13.76 ± 1.27	0.66 ± 0.02	18.6 ± 1.6 (20.5)
	C_{60}	0.51 ± 0.06	13.13 ± 1.53	0.33 ± 0.04	5.8 ± 1.6 (7.4)
	C_{70}	0.24 ± 0.06	13.05 ± 2.84	0.30 ± 0.05	2.1 ± 0.6 (2.7)
600 lux					
	Two-step PCBM	0.83 ± 0.02	79.55 ± 2.51	0.74 ± 0.02	25.1 ± 1.2 (26.4)
	One-step PCBM	0.73 ± 0.01	81.00 ± 2.52	0.75 ± 0.02	23.1 ± 1.2 (24.8)
	C_{60}	0.66 ± 0.05	65.88 ± 3.58	0.51 ± 0.03	11.6 ± 1.8 (13.6)
	C_{70}	0.53 ± 0.04	61.53 ± 5.73	0.40 ± 0.01	6.5 ± 0.9 (7.9)
1000 lux					
	Two-step PCBM	0.84 ± 0.01	132.26 ± 5.19	0.75 ± 0.02	26.3 ± 1.1 (27.4)
	One-step PCBM	0.76 ± 0.01	133.96 ± 4.63	0.76 ± 0.01	24.8 ± 1.2 (26.0)
	C_{60}	0.70 ± 0.04	108.77 ± 6.04	0.57 ± 0.04	13.7 ± 1.5 (15.5)
	C_{70}	0.57 ± 0.05	104.57 ± 6.39	0.46 ± 0.03	8.3 ± 1.1 (10.0)

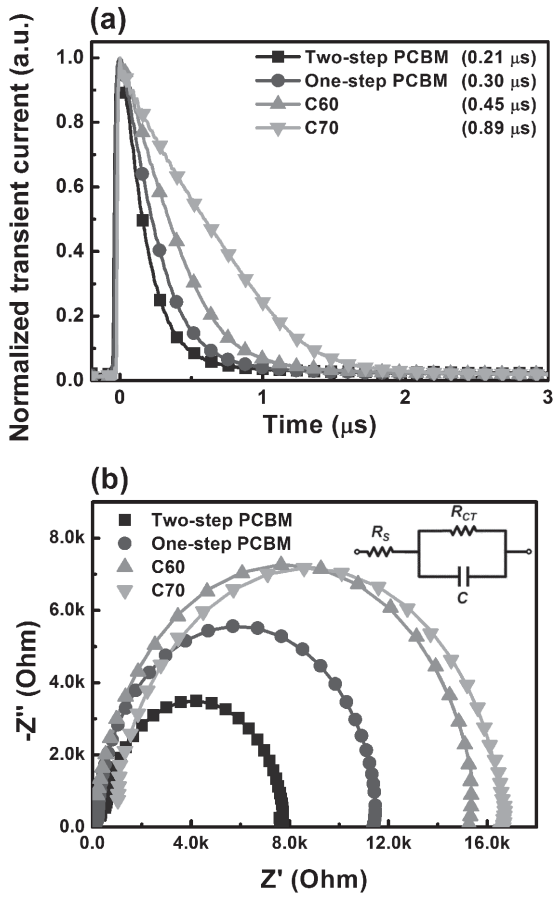

Figure 4. a) Normalized transient photocurrent measurement results of PePVs with different ETLs. The numbers in the parentheses show the transient time. b) Nyquist plots of PePVs with different ETLs, where the symbols and solid lines represent the measured data and fitting results, respectively.

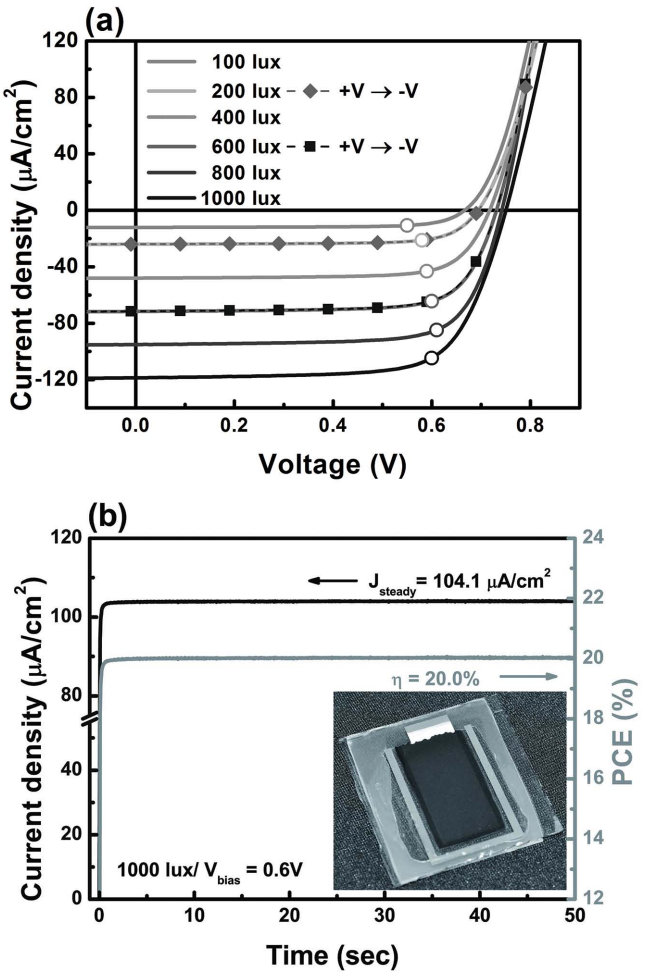

Figure 5. a) *J–V* characteristics of a large-area PePV (5.44 cm^2) under indoor illumination. The solid lines and dashed lines represent the scanning direction from negative to positive bias and from positive to negative bias, respectively. b) Photocurrent density and PCE as a function of time of the large-area PePV held at bias of MPP (0.6 V). Inset: photograph of the large-area PePV.

A more clear effect can be observed in the V_{OC} versus light intensity curves in Figure S3 (Supporting Information).[46] The one-step and two-step PCBM cells have slopes of 1.54 kT/q and 1.47 kT/q, respectively, which fall in the 1–2 kT/q category usually observed in solar cells operated under bright-light conditions.[47–49] The two-step PCBM device clearly showed the least recombination behavior. However, the C_{60} and C_{70} ETL devices exhibit a steep decrease of V_{OC} with decreasing incident light intensity. The results indicate that the C_{60} and C_{70} ETL devices exhibited much higher trap densities than the critical trap density and that the device behavior can no longer be predicted using the simple diode equation.[50]

2.3. Large Device Characterization

A large-area device with the optimized structure and a device area of 5.44 cm^2 was fabricated, and its properties were measured; the results are presented in **Figure 5**a. Compared with the small-area device, the large-area cell only exhibited a small efficiency decrease, and the device exhibited a decent PCE of 18.6%–20.4% from 100 lux to 1000 lux. As observed in Figure 5b, the device can deliver a steady power of 340 μW under 1000 lux illumination, which is readily sufficient for the modern sensing nodes of IoT.[51–54] The performance of the large-area device is further compared with the commercially available state-of-the-art designed-for-dim-light application DSSCs (active area = 1 cm^2) and OSCs (active area = 2.5 cm^2) in Figure S2 (Supporting Information). The PePVs exhibited better performance even with a larger device area. The long time stability of the large-area device was also measured by storing the device in a normal indoor environment with regular testing for 40 days. As observed in Figure S4 (Supporting Information), the device maintained ≈97% of its peak efficiency after 40 days with only a simple UV–epoxy encapsulation without using any desiccant. Since the photoexcitation stress is much lower in the dim-light condition, we believe the slight efficiency roll-off was mainly due to the extrinsic factors (e.g., H_2O, O_2).[55] Improved stability is anticipated if a further optimized encapsulation technique is incorporated with the cells.

3. Conclusion

In summary, the use of PV cells with an organometallic perovskite as the active layer for indoor dim-light energy harvesting has been evaluated. By carefully designing the ETL materials and fabrication processes, the traps in the perovskite active layers and carrier dynamics could be controlled, and efficient devices were demonstrated. The best-performing small-area PePVs exhibited a promising high PCE up to ≈27.4%, no hysteresis behavior, and a small ΔV_{MPP} of ≈0.1 V under fluorescent lamp illumination at 100–1000 lux. The large-area device also exhibited a high PCE of 20.4% and a promising long-term stability. Compared with the most efficient III–V solar cells, DSSCs, and OSCs, the competitive efficiency, low fabrication cost, and low raw material costs make PePVs ideal for indoor light harvesting and as IoT power provider. Moreover, there is still room for further improvement in both the efficiency and stability via bandgap engineering of the perovskite materials, optimization of the fabrication process and device structure, and improved encapsulation.

4. Experimental Section

Device Preparation: Methylammonium iodide (MAI) was synthesized as reported elsewhere in the literature. Precleaned ITO-coated glass was used as the substrate. PEDOT:PSS (Clevios AI4083) was spin-coated on UV–ozone pretreated ITO glass, followed by thermal annealing at 135 °C for 30 min. The perovskite precursor solution of 40 wt% was prepared by mixing the PbI_2, $PbCl_2$, and MAI (at a molar ratio of 5:3:14) in dimethylformamide at 60 °C for 24 h. The perovskite precursor solution was then spin-coated onto the 60 °C ITO/PEDOT:PSS substrate at 8000 rpm for 60 s before being annealed at 100 °C for 10 min. For the C_{60} and C_{70} ETL devices, the substrates were cooled down to room temperature and loaded into a high vacuum (base pressure ≈ 2×10^{-6} Torr) to deposit 120 nm of C_{60} or C_{70} at a constant rate of 1 Å s^{-1} via thermal evaporation. For the one-step PCBM ETL devices, after cooling the perovskite film to room temperature, a dense PCBM solution (dissolved in a mixture of chlorobenzene and chloroform (1:1, v/v), 30 mg mL^{-1}) was spin-coated on the ITO/PEDOT:PSS/perovskite substrate at 1500 rpm for 60 s. For the two-step PCBM ETL devices, the perovskite films were first annealed at 100 °C for 2 min after spin-coating the perovskite film and rapidly transferred to the spin-coater. A dilute PCBM solution (dissolved in chlorobenzene, 3 mg mL^{-1}) was spin-coated on the film at 1500 rpm for 60 s. Then, the substrate was immediately transferred back to the 100 °C hot plate and annealed for 8 min. Next, a dense PCBM solution (dissolved in chlorobenzene and chloroform (1:1, v/v), 30 mg mL^{-1}) was spin-coated at 1500 rpm for 60 s. TmPyPB (7 nm) and silver (150 nm) were deposited on the fullerene ETLs via thermal evaporation as the electron-transporting buffer layer and the cathode, respectively. Finally, the devices were encapsulated using a UV-cured sealant (Everwide Chemical Co., Epowide EX) and a cover glass under an anhydrous nitrogen atmosphere and subsequently characterized in air. The device area was defined by a mask with an area of 5.1 mm^2 for the small-area devices and of 5.44 cm^2 for the large-area devices.

Characterization: The samples for the SEM measurements were prepared using the same conditions as those used for the device fabrication, and the SEM images were obtained using a Hitachi SU8010 field-emission scanning electron microscope. The *J–V* characteristics of the devices were measured using a Keithley 2636A SourceMeter in the dark and under 6500 K color temperature Philips T5 fluorescent lamp illumination. Normally, the scan direction was from negative to positive bias. The irradiance and luminance were determined using a NIST-traceable OPHIR radiometer (PD300-BB-50 mW) and a photometer (PD300-CIE), respectively. Impedance spectroscopy measurements were performed using an Autolab PGSTAT 128N equipped (Eco-chemie, Netherland) with FRA module; the frequency was swept over the range of 10 mHz to 100 kHz. Transient photocurrent measurements were conducted in the dark using the second harmonic of a Nd:YAG laser (532 nm) as an excitation source. The transient signals were amplified using a FEMTO variable-gain high-speed current amplifier (DHPCA-100) and were recorded using a Tektronix oscilloscope (DPO3050). Averages of 256 traces were calculated to improve the signal-to-noise ratio. The commercial DSSC (G1, active area = 1 cm^2) and OSC (150306M1, active area = 2.5 cm^2) submodules were purchased from Taiwan DSC PV and Raynergy Tek Inc. (Taiwan), respectively.

Supporting Information

Supporting Information is available from the Wiley Online Library or from the author.

Acknowledgements

The authors would like to acknowledge the financial support from the Ministry of Science and Technology of Taiwan (Grant Nos. 104-2112-M-007-019, 102-2221-E-007-125-MY3, 103-2633-M-007-001) and National Tsing Hua University.

Received: August 16, 2015
Revised: September 14, 2015
Published online: October 15, 2015

[1] J. Gubbi, R. Buyya, S. Marusic, M. Palaniswami, *Future Gener. Comput. Syst.* **2013**, *29*, 1645.
[2] D. Miorandi, S. Sicari, F. De Pellegrini, I. Chlamtac, *Ad Hoc Netw.* **2012**, *10*, 1497.
[3] L. Atzori, A. Iera, G. Morabito, *Comput. Netw.* **2010**, *54*, 2787.
[4] B. Warneke, B. Atwood, K. S. J. Pister, in *IEEE 40th Int. Conf. on Micro Electro Machanical Systems*, IEEE, Piscataway, NJ, USA **2001**, 357.
[5] R. Steim, T. Ameri, P. Schilinsky, C. Waldauf, G. Dennler, M. Scharber, C. J. Brabec, *Sol. Energy Mater. Sol. Cells* **2011**, *95*, 3256.
[6] A. Fakharuddin, R. Jose, T. M. Brown, F. Fabregat-Santiago, J. Bisquert, *Energy Environ. Sci.* **2014**, *7*, 3952.
[7] J. Gong, S. B. Darling, F. You, *Energy Environ. Sci.* **2015**, *8*, 1953.
[8] A. Kojima, K. Teshima, Y. Shirai, T. Miyasaka, *J. Am. Chem. Soc.* **2009**, *131*, 6050.
[9] A. Wakamiya, M. Endo, T. Sasamori, N. Tokitoh, Y. Ogomi, S. Hayase, Y. Murata, *Chem. Lett.* **2014**, *43*, 711.
[10] N.-G. Park, *J. Phys. Chem. Lett.* **2013**, *4*, 2423.
[11] N.-G. Park, *Nat. Mater.* **2015**, *14*, 140.
[12] K.-G. Lim, H.-B. Kim, J. Jeong, H. Kim, J. Y. Kim, T.-W. Lee, *Adv. Mater.* **2014**, *26*, 6461.
[13] Y. H. Hu, *Adv. Mater.* **2014**, *26*, 2102.
[14] J.-W. Lee, D.-J. Seol, A.-N. Cho, N.-G. Park, *Adv. Mater.* **2014**, *26*, 4991.
[15] K. M. Boopathi, M. Ramesh, P. Perumal, Y.-C. Huang, C.-S. Tsao, Y.-F. Chen, C.-H. Lee, C.-W. Chu, *J. Mater. Chem. A* **2015**, *3*, 9257.
[16] M. Freunek, M. Freunek, L. M. Reindl, *IEEE J. Photovolt.* **2013**, *3*, 59.
[17] R. Mirhosseini, M. F. Schubert, S. Chhajed, J. Cho, J. K. Kim, E. F. Schubert, *Opt. Express* **2009**, *17*, 10806.
[18] Y. Shao, Z. Xiao, C. Bi, Y. Yuan, J. Huang, *Nat. Commun.* **2014**, *5*, 5784.

[19] N. Marinova, W. Tress, R. Humphry-Baker, M. I. Dar, V. Bojinov, S. M. Zakeeruddin, M. K. Nazeeruddin, M. Grätzel, *ACS Nano* **2015**, *9*, 4200.
[20] Q. Chen, H. Zhou, T.-B. Song, S. Luo, Z. Hong, H.-S. Duan, L. Dou, Y. Liu, Y. Yang, *Nano Lett.* **2014**, *14*, 4158.
[21] H.-W. Lin, C.-W. Lu, L.-Y. Lin, Y.-H. Chen, W.-C. Lin, K.-T. Wong, F. Lin, *J. Mater. Chem. A* **2013**, *1*, 1770.
[22] J.-Y. Jeng, Y.-F. Chiang, M.-H. Lee, S.-R. Peng, T.-F. Guo, P. Chen, T.-C. Wen, *Adv. Mater.* **2013**, *25*, 3727.
[23] J. H. Heo, H. J. Han, D. Kim, T. K. Ahn, S. H. Im, *Energy Environ. Sci.* **2015**, *8*, 1602.
[24] C.-W. Chen, H.-W. Kang, S.-Y. Hsiao, P.-F. Yang, K.-M. Chiang, H.-W. Lin, *Adv. Mater.* **2014**, *26*, 6647.
[25] J. Xu, A. Buin, A. H. Ip, W. Li, O. Voznyy, R. Comin, M. Yuan, S. Jeon, Z. Ning, J. J. McDowell, P. Kanjanaboos, J.-P. Sun, X. Lan, L. N. Quan, D. H. Kim, I. G. Hill, P. Maksymovych, E. H. Sargent, *Nat. Commun.* **2015**, *6*, 7081.
[26] C. Bi, Q. Wang, Y. Shao, Y. Yuan, Z. Xiao, J. Huang, *Nat. Commun.* **2015**, *6*, 7747.
[27] W. Tress, N. Marinova, T. Moehl, S. M. Zakeeruddin, M. K. Nazeeruddin, M. Grätzel, *Energy Environ. Sci.* **2015**, *8*, 995.
[28] J. M. Frost, K. T. Butler, A. Walsh, *APL Mater.* **2014**, *2*, 081506.
[29] C. Zhao, B. Chen, X. Qiao, L. Luan, K. Lu, B. Hu, *Adv. Energy Mater.* **2015**, *5*, 1500279 .
[30] A. S. Teran, W. Joeson, L. Wootaek, K. Gyouho, L. Yoonmyoung, D. Blaauw, J. D. Phillips, *IEEE Trans. Electron. Devices* **2015**, *62*, 2170.
[31] I. Mathews, G. Kelly, P. J. King, R. Frizzell, in *IEEE 40th Photovoltaic Specialist Conf.*, IEEE, Piscataway, NJ, USA **2014**, 0510.
[32] T. Esram, P. L. Chapman, *IEEE Trans. Energy Convers.* **2007**, *22*, 439.
[33] N. Onat, *Int. J. Photoenergy* **2010**, *2010*, 1.
[34] M. Orabi, F. Hilmy, A. Shawky, J. A. Abu Qahouq, E.-S. Hasaneen, E. Gomaa, *Sol. Energy* **2015**, *117*, 10.
[35] M. T. Penella, M. Gasulla, *Int. J. Photoenergy* **2014**, *2014*, 7.
[36] M. Vincheh, A. Kargar, G. Markadeh, *Arab. J. Sci. Eng.* **2014**, *39*, 4715.
[37] Y. Liu, Q. Chen, H.-S. Duan, H. Zhou, Y. Yang, H. Chen, S. Luo, T.-B. Song, L. Dou, Z. Hong, Y. Yang, *J. Mater. Chem. A* **2015**, *3*, 11940.
[38] H. Zhou, Q. Chen, G. Li, S. Luo, T.-b. Song, H.-S. Duan, Z. Hong, J. You, Y. Liu, Y. Yang, *Science* **2014**, *345*, 542.
[39] C. Motta, F. El-Mellouhi, S. Sanvito, *Sci. Rep.* **2015**, *5*, 12746.
[40] S. Kobayashi, T. Takenobu, S. Mori, A. Fujiwara, Y. Iwasa, *Sci. Technol. Adv. Mater.* **2003**, *4*, 371.
[41] E. von Hauff, V. Dyakonov, J. Parisi, *Sol. Energy Mater. Sol. Cells* **2005**, *87*, 149.
[42] X. Wu, M. T. Trinh, D. Niesner, H. Zhu, Z. Norman, J. S. Owen, O. Yaffe, B. J. Kudisch, X. Y. Zhu, *J. Am. Chem. Soc.* **2015**, *137*, 2089.
[43] A. Abate, M. Saliba, D. J. Hollman, S. D. Stranks, K. Wojciechowski, R. Avolio, G. Grancini, A. Petrozza, H. J. Snaith, *Nano Lett.* **2014**, *14*, 3247.
[44] K. Wang, C. Liu, P. Du, J. Zheng, X. Gong, *Energy Environ. Sci.* **2015**, *8*, 1245.
[45] Y. Xiao, G. Han, Y. Chang, H. Zhou, M. Li, Y. Li, *J. Power Sources* **2014**, *267*, 1.
[46] S. R. Cowan, A. Roy, A. J. Heeger, *Phys. Rev. B* **2010**, *82*, 245207.
[47] H.-C. Ting, Y.-H. Chen, L.-Y. Lin, S.-H. Chou, Y.-H. Liu, H.-W. Lin, K.-T. Wong, *ChemSusChem.* **2014**, *7*, 457.
[48] M. M. Mandoc, F. B. Kooistra, J. C. Hummelen, B. de Boer, P. W. M. Blom, *Appl. Phys. Lett.* **2007**, *91*, 263505.
[49] W. Nie, H. Tsai, R. Asadpour, J.-C. Blancon, A. J. Neukirch, G. Gupta, J. J. Crochet, M. Chhowalla, S. Tretiak, M. A. Alam, H.-L. Wang, A. D. Mohite, *Science* **2015**, *347*, 522.
[50] J. C. Blakesley, D. Neher, *Phys. Rev. B* **2011**, *84*, 075210.
[51] C. C. Enz, A. El-Hoiydi, J. D. Decotignie, V. Peiris, *Computer* **2004**, *37*, 62.
[52] H. Yu-Jie, T. Te-Hsuen, L. Tzu-Wei, H. Che-Wei, Y. Pei-Wen, K. Po-Hung, L. Chih-Ting, L. Shey-Shi, *IEEE J. Solid-State Circuits* **2014**, *49*, 851.
[53] Z. Wang, Y. Liu, Y. Sun, Y. Li, D. Zhang, H. Yang, in *IEEE Int. Symp. on Circuits and Systems*, IEEE, Piscataway, NJ, USA **2015**, 2301.
[54] A. Burdett, *IEEE Solid State Circuits Mag.* **2015**, *7*, 18.
[55] Y.-H. Kim, H. Cho, J. H. Heo, T.-S. Kim, N. Myoung, C.-L. Lee, S. H. Im, T.-W. Lee, *Adv. Mater.* **2015**, *27*, 1248.